

Nitrogen-doped Porous Carbon Derived from Chitin with Enhanced Performances for Oxygen Reduction Reaction and Supercapacitor

Lei Yao^{1,2}, Wenhua Zhong², Lei Qiu² and Libo Deng^{2,*}

¹ College of Environmental Sciences and Engineering, Peking University, The Key Laboratory of Water and Sediment Sciences, Ministry of Education, Beijing 100871, China

² College of Chemistry and Environmental Engineering, Shenzhen University, Shenzhen 518060, China

*E-mail: Denglb@szu.edu.cn

Received: 17 February 2018 / Accepted: 10 April 2018 / Published: 10 May 2018

Herein a porous carbon with a high content of nitrogen, high surface area and high degree of graphitization was prepared by pyrolysing a cheap and abundant biopolymer chitin in the presence of both FeCl₃ and ZnCl₂. It was found the electrochemical performance is significantly dependent on the carbonization temperature. The 1000 °C-treated carbon exhibited high electrocatalytic activity as catalysts for oxygen reduction reaction (ORR), showing a four-electron oxygen reduction pathway with an onset potential of 0.978 V (against reversible hydrogen electrode, RHE). The porous carbon also exhibited a capacitance of 130 F/g at 0.5A/g and excellent rate performance as electrode for supercapacitors. These results are attributed to the high surface area, as well as the high degree of graphitization which endows the as-prepared carbon with a high electrical conductivity.

Keywords: Biomass, porous carbon, chitin, oxygen reduction reaction, supercapacitor

1. INTRODUCTION

Carbonaceous materials have been considered as promising candidates for ORR electrocatalysts used in fuel cells and metal-air batteries, as well as electrodes in supercapacitors due to their excellent chemical stability and low cost [1, 2]. Particularly, porous carbons derived from biomass have been attracting tremendous attention for their potential applications in electrochemical energy storage and conversion recently [3-7]. To name a few, carbons prepared from bamboo fungus and collagen showed high electrocatalytic activity towards ORR [8, 9], and those derived from coconut shells, leaves and lotus also exhibited outstanding capacitive performance in supercapacitors [10-12].

For both of the aforementioned electrochemical applications, the prerequisites for high-performance carbons are large accessible surface areas, highly conductive, good wettability and sufficient electrochemically active centers [13]. To this end, various approaches have been developed to optimize the composition, chemical state and microstructure of the biomass-derived carbons [14, 15]. Among them, doping with heteroatoms and increasing the graphitization degree using graphitization catalysts during the carbonization process are particularly effective [16]. For example, nitrogen and sulfur have been doped into porous carbon through a two-step process, i.e. firstly pyrolysis of biomass and followed by heat treatment with thiourea [17]. On the other hand, highly graphitized carbons have been prepared by methods such as chemical vapor deposition on catalysts (e.g. MgO and Cu), followed by removing the catalysts [18, 19]. However, these processes are tedious and time consuming. Moreover, it is still a great challenge to obtain a highly graphitized structure while maintaining a high surface area simultaneously in porous carbons. More facile methods are needed to control the microstructure and foster the practical application of biomass-derived carbons.

In our previous study, a porous carbon was prepared by carbonization of chitin (a biopolymer extracted from e.g. crab and shrimp) at 800 °C in the presence of FeCl₃ and ZnCl₂ [20]. When used directly as electrocatalysts for ORR, the as-prepared carbon exhibited poor performance due to encapsulation of the catalytic active centers by the amorphous carbon and the existence of less active iron compounds. The catalytic performance of the porous carbon was then enhanced significantly by etching with air plasma which removes the less active carbon domains and change the chemical state of the residual iron compounds. In this study, we demonstrate that high catalytic performance can be also achieved by treating chitin at a higher temperature (1000 °C) instead of etching by plasma. Furthermore, the as-prepared carbon also exhibited excellent capacitive performance as electrodes for supercapacitors.

2. EXPERIMENTAL

2.1 Preparation of porous carbon

The porous carbon was prepared following the procedure described in our previous study [20]. Specifically, the commercial chitin polymer (Sigma-Aldrich) was first heat-treated at 240 °C in air for 2 h, which was then mixed with FeCl₃ and ZnCl₂ with a mass ratio of 1:3:3. Subsequently, the mixture was heated to 1000 °C in nitrogen at a ramp rate of 5 °C/min and kept for 2h. The mixture was leached thoroughly with 2M hydrochloric acid and washed with deionized water to give the porous carbon which is denoted as PC-1000. The carbon obtained with a similar process, changing only the carbonization temperature to 800 °C is denoted as PC-800.

2.2 Characterization

The morphology and microstructure of were characterized using a JSM-7800F scanning electron microscopy (SEM) and a JEM-2100 transmission electron microscopy (TEM), respectively. X-ray diffractometer (XRD, $\lambda = 1.54 \text{ \AA}$, CuK α radiation) was performed on a Philips X'PERT APD

powder. Raman spectroscopy was performed on a Renishaw Invia Reflex system. The surface area was measured using nitrogen adsorption (Belsorp-max). X-ray photoelectron spectroscopy (XPS) measurements were performed on an Ultra DLD using a monochromic Al X-ray source.

2.3 Electrocatalytic activity measurement

To prepare working electrode for electrocatalytic measurement, the carbon was dispersed in ethanol at a concentration of 1 mg mL^{-1} by sonication. Desired volume of Nafion was added into the dispersion to make a concentration of 0.5%. The dispersion was then coated onto a glassy carbon (GC) electrode and dried thoroughly. The loading of active material on the electrode was 0.28 mg/cm^2 .

Measurements were carried out in a three-electrode cell containing 0.1 M KOH solution as the electrolyte, and using an Ag/AgCl electrode as the reference electrode and a Pt foil as the counter electrode. Cyclic voltammogram (CV) measurements were conducted at a scan rate of 10 mV s^{-1} from -0.8 to +0.2 V (vs Ag/AgCl). Linear sweep voltammogram (LSV) measurements were performed on rotating disk electrode (RDE) which was controlled by an RRDE-3A system (ALS, Japan), with a scan rate of 10 mV/s . The potential measured against the Ag/AgCl electrode was converted to a potential versus RHE according to $E (\text{vs. RHE}) = E (\text{vs. Ag/AgCl}) + 0.197 + 0.059\text{pH}$ [20].

2.4 Capacitance measurement

The capacitive performance was assessed using a two-electrode configuration by assembling the carbons into coin-cell supercapacitors, which were described in our previous studies [21-23]. Specifically, desired amount of carbon was mixed with carbon black and polytetrafluoroethene with a mass ratio of 80:10:10. The mixture was ground in ethanol to form a paste, which was then casted onto nickel foam, dried thoroughly and pressed to obtain thin and rigid electrodes. Two pieces of electrodes, separated with a cellulosic film which was impregnated with 6 M KOH solution, were then assembled into supercapacitors. The performance was then tested using CV, galvanostatic charge/discharge and electrochemical impedance spectroscopy (EIS) methods.

3. RESULTS AND DISCUSSION

3.1 Materials characterization

Chitin was selected as the carbon source as it is abundant, renewable and nitrogen-rich which can be inherited in the pyrolyzed carbon. Furthermore, the chemical structure of chitin is similar to cellulose which is known for its ability to convert into graphitic structure [24]. ZnCl_2 was used as the activation agent to obtain a high surface area herein. Porous flakes with pore sizes in the range of 10-50 nm can be seen from the SEM images for the pyrolyzed carbon (Figure 1a and 1b). The high porosity was created by chemical activation with ZnCl_2 which promotes dehydration, charring and aromatization of the precursor during carbonization [25].

The microstructure was inspected using TEM. Crystalline domain with low structural order can be seen from the TEM image (bottom left in Figure 1c), suggesting a relatively high graphitization degree for this material. The graphitic structure is thought to be related to the chemical structure of chitin which can rearrange into hexagonal carbon rings and further into crystallites. This microstructure is also associated with the catalytic graphitization of FeCl_3 which (in the form of Fe or Fe-based compounds) serves as a template for crystallization of carbon [26]. Nanodots with an average diameter of 5 nm are distributed in the carbon matrix (Figure 1c and 1d), which are identified as iron-containing nanoparticles [20]. These particles, although with a low concentration, are effective in improving the electrocatalytic activity.

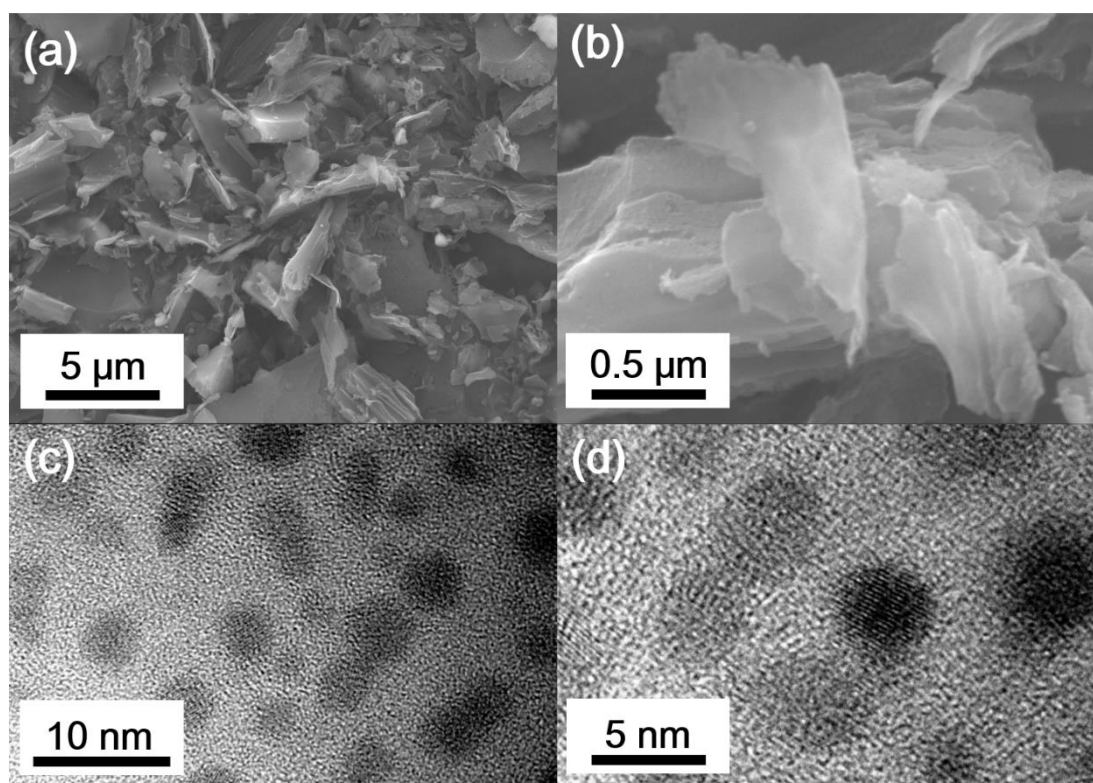


Figure 1. (a) and (b): SEM images; (c) and (d): TEM images for PC-1000.

The relatively high degree of graphitization was confirmed by XRD characterization. A broad but strong peak is seen at 26° for PC-1000 (Figure 2a), corresponding to (002) plane of graphite crystallites. The broad diffraction indicates polycrystalline nature of this material. However, this peak is already narrower than that for PC-800, indicating the increase of crystallinity with the increase of carbonization temperature for these carbons. The relatively good crystallinity and structural order is also revealed by Raman spectroscopic analysis (Figure 2b). It was found the intensity ratio between the D-band (centered at $\sim 1350 \text{ cm}^{-1}$) and G-band (centered at $\sim 1580 \text{ cm}^{-1}$), I_D/I_G , decreased from 1.02 to 0.92 as the temperature increased from 800°C to 1000°C , suggesting the decrease of defects and increase of structural order in PC-1000. The increase of I_D/I_G ratio is also accompanied with the

decrease of full-width at half maximum of both D- and G- bands, further confirming the increase of structural order of the carbon with the increase of carbonization temperature [27].

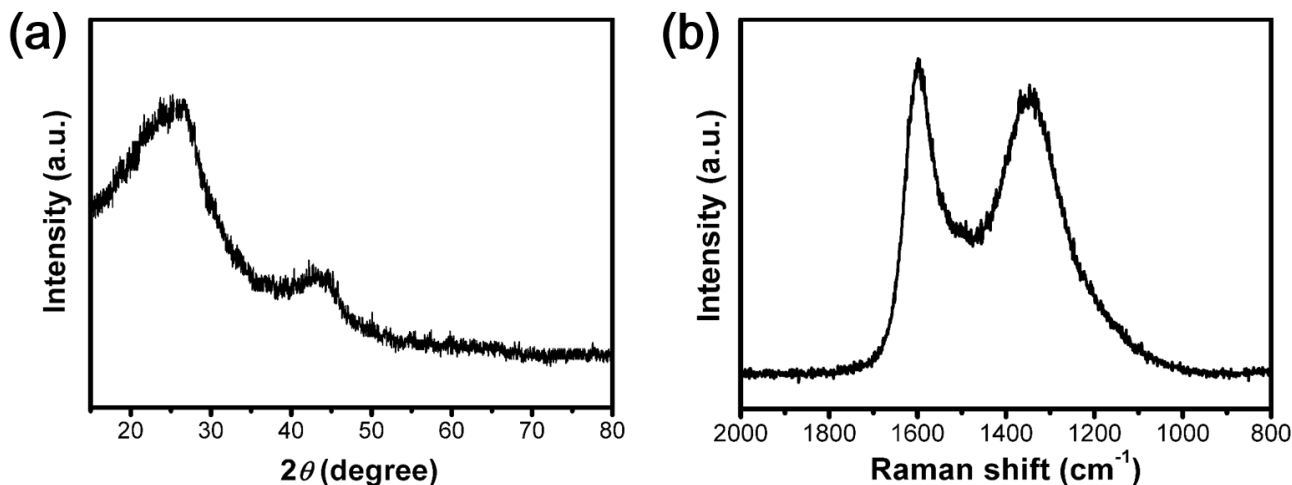


Figure 2. (a) XRD patterns and (b) Raman spectra for PC-1000.

The Brunauer- Emmett- Teller (BET) surface area and pore size distribution were investigated by nitrogen adsorption/desorption. The obtained isotherm as shown in Figure 3 reveals a typical type-I curve, indicating these carbons contain abundant micropores. An extraordinary specific surface area, of 2305 cm²/g is obtained for this material, which is even higher than that prepared at 800 °C (i.e. 1730 cm²/g) [20]. This can be understood that more hydrogen, oxygen and nitrogen atoms were removed in the form of gas at a higher temperature, which creates more micropores in the carbon matrix. The pore size distribution is estimated using a non-local density functional theory (NLDFT) and shown in Figure 3b. The average diameters is 1.7 nm for PC-1000, which confirms the microporous nature of these carbons.

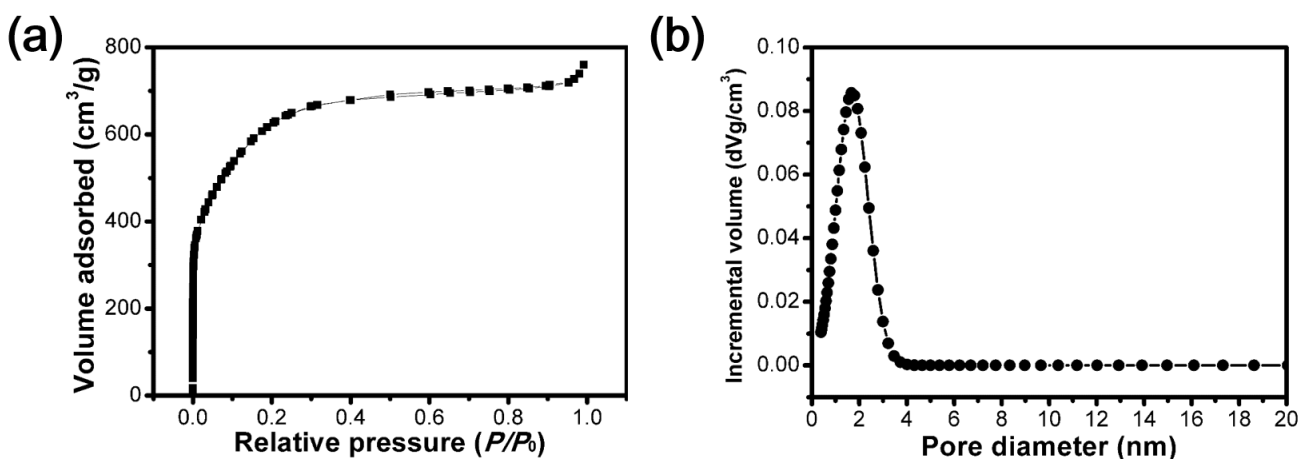


Figure 3. (a) Nitrogen adsorption/desorption and (b) pore size distribution PC-1000.

The composition of the pyrolyzed carbon also changed with the increase of carbonization temperature. For PC-1000, the atomic percentage for carbon, oxygen, nitrogen and iron elements as determined using XPS (Figure 4) are 86.62%, 10.41%, 2.70% and 0.27%, and the corresponding values for PC-800 are 80.58%, 11.43%, 7.15% and 0.84% (reported in previous study [20]), respectively. It will be shown later the decrease of contents of heteroatoms (i.e. O, N and Fe) with the carbonization temperature did not deteriorate but instead enhanced the electrocatalytic activity, signifying the primary role of graphitization degree and surface area on the electrochemical performance.

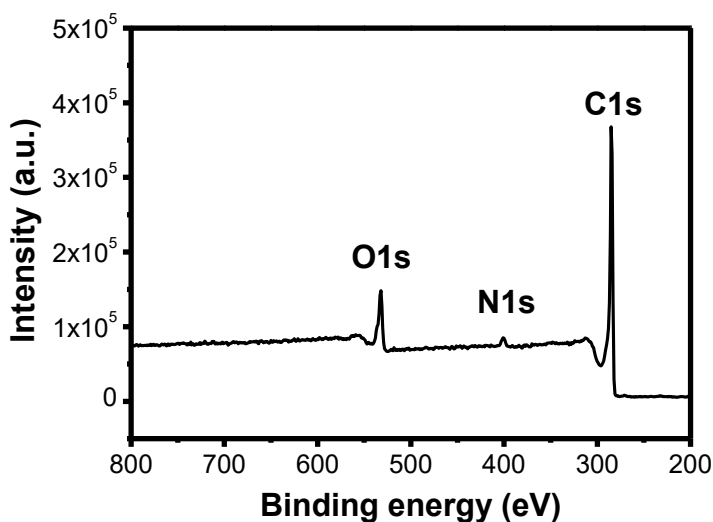


Figure 4. The XPS spectrum for PC-1000.

3.2 Catalytic performance for ORR

The large surface area and high level of nitrogen and iron co-doping in PC-1000 make it promising for electrocatalytic ORR application. This activity is evident from the CV curve acquired in O_2 -saturated KOH solution where an obvious reduction peak can be seen at 0.81 V (Figure 5a). In contrast, the curve obtained from N_2 -saturated KOH solution showed no reduction reaction. The electrocatalytic kinetics were then investigated by RDE voltammograms. Figure 5b shows the LSV curves obtained at different rotating speeds. The onset potential, defined as the potential at 5% of the limiting diffusion current, was 0.979 V for PC-1000, which is similar to that of PC-800 reported in our previous study [20]. The number of electron transferred during the reduction reaction, n , was calculated using the Koutecky-Levich equations [28], which is around 3.84 (varies only slightly) in the potential range of 0.3-0.5 V (Figure 5c). This value is significantly higher than that of PC-800 (i.e. 2.8), and suggests that the ORR promoted by PC-1000 occurs through a four-electron process. The performance as characterized by the onset potential and transferred electrons for PC-1000 is comparable to the good results reported in literatures (see Table 1) for carbon-based ORR electrocatalysts [13, 29, 30].

Table 1. The electrocatalytic performance toward ORR for different carbonaceous materials

| Material | Onset potential (V, vs RHE) | Transferred electrons | Reference |
|--|-----------------------------|-----------------------|-----------|
| Wood-derived carbon | 0.98 | 3.89 | [13] |
| Citric acid and dicyandiamide-derived carbon | -- | 3.89 | [29] |
| Cellulose nanoribbon-derived carbon | 0.904 | 3.84 | [30] |
| Bean dreg-derived carbon | 0.945 | 3.78 | [31] |
| Chitin-derived carbon (PC-1000) | 0.979 | 3.84 | This work |

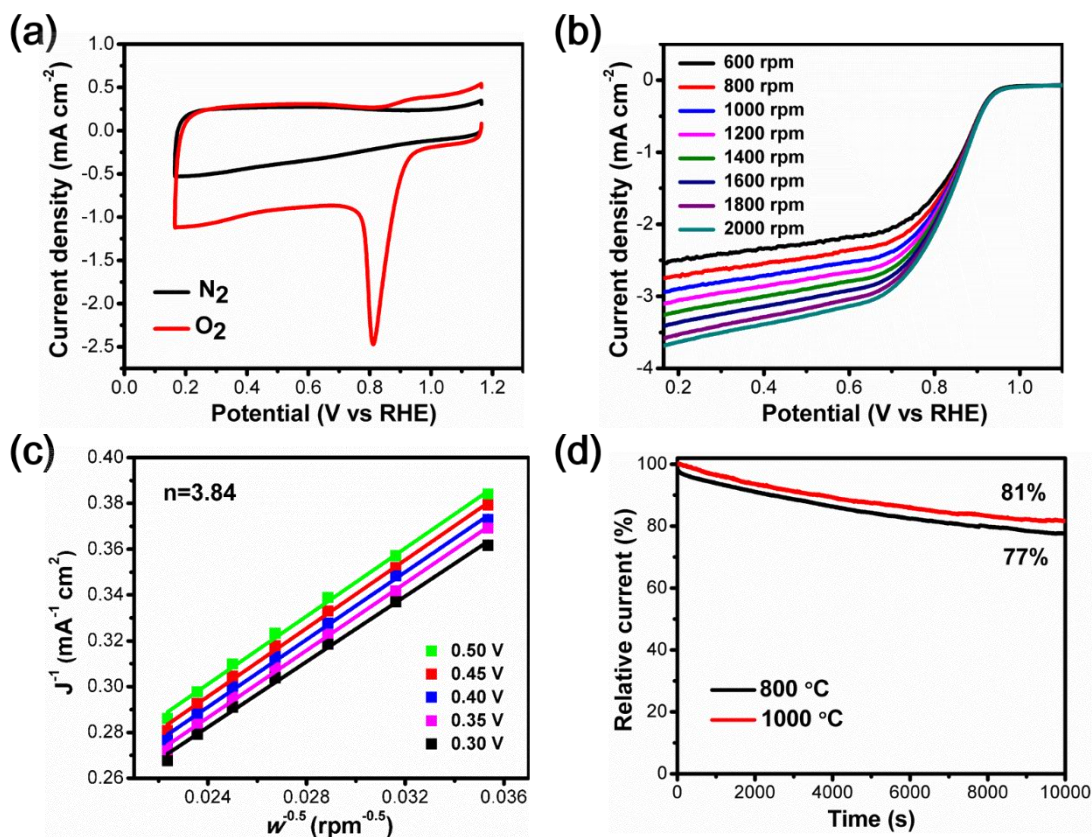


Figure 5. Electrocatalytic performance for PC-1000: (a) CV curves measured in N₂ and O₂ saturated 0.1 M KOH solution; (b) LSV curves measured at different rotating speeds; (c) the Koutecky-Levich plots at different potentials; (d) the current retention during the long-term catalytic process for both PC-800 and PC-1000.

Furthermore, the limiting current also increased from 3.15 mA/cm² for PC-800 to 3.61 mA/cm² for PC-1000. The durability of the chitin-derived carbons was further tested by measuring the variation of current over a long duration at 0.36 V. The PC-800 retained 77% of its initial current after 10000 s of service, whereas the current retention is 81% for PC-1000 which is superior to the commercial Pt/C electrocatalyst (i.e. 75%) tested under the same condition. These results suggest the electrocatalytic performance of the 800 °C-treated carbon can be significantly enhanced by treating at 1000 °C, similar to the effect of plasma etching on the catalytic performance. This enhancement is due to a higher degree of graphitization (and consequently a higher conductivity as revealed by impedance measurement discussed later), as well as the increase of specific surface area which could expose more catalytic active centers.

3.3 Electrochemical capacitance

The as-prepared carbons might also be suitable for supercapacitor application due to their high surface area. To examine their capacitive performance, the carbons were pressed into nickel foam and two such electrodes were assembled into symmetric coin-cell capacitors. All CV curves for both PC-800 and PC-1000 exhibit rectangular like loops with only slight distortion at 100 mV/s (closer inspection discloses that the distortion is even less for PC-1000 than for PC-800, see Figure 6a and 6c), suggesting typical electrical double layer capacitance with fast ion-transport capability, i.e. excellent conductivity. No obvious redox peaks or pseudocapacitance was observed due to the low content of iron compounds.

Table 2. The capacitive performance for different carbonaceous materials (using KOH as electrolyte unless otherwise stated)

| Material | Current density (A/g) | Capacitance (F/g) | Reference |
|---------------------------------|-----------------------|---------------------------------|-----------|
| Sucrose-derived carbon | 0.1 | 133 | [33] |
| Alkynyl carbon | 0.1 | 133.4 | [34] |
| Cattail-derived carbon | 0.5 | 126.5 | [35] |
| Pistachio shell-derived carbon | 20 mV/s | ~110 (0.1 M NaNO ₃) | [36] |
| Chitin-derived carbon (PC-1000) | 0.5 | 130 | This work |

The galvanostatic charge/discharge curves show isosceles triangles with no appreciable voltage drop (Figure 6b and 6d), again indicating the excellent conductivity in these electrodes. The specific capacitance C_{sp} for each electrode is calculated according to the equation [32]:

$$C_{sp} = 4 \times \frac{I}{m \times (dV/dt)} \quad (1)$$

where I is the constant charge/discharge current, t is the discharge time, V is the potential during the discharge process and m is the total mass of active materials in the two electrodes. The capacitances at

a current density of 0.5 A/g was 99 F/g for PC-800 and increased markedly to 130 F/g for PC-1000 which is comparable with the good results (see Table 2) for carbonaceous electrode materials [16, 33-35]. The capacitance enhancement is also related to the higher degree of graphitization and larger surface area.

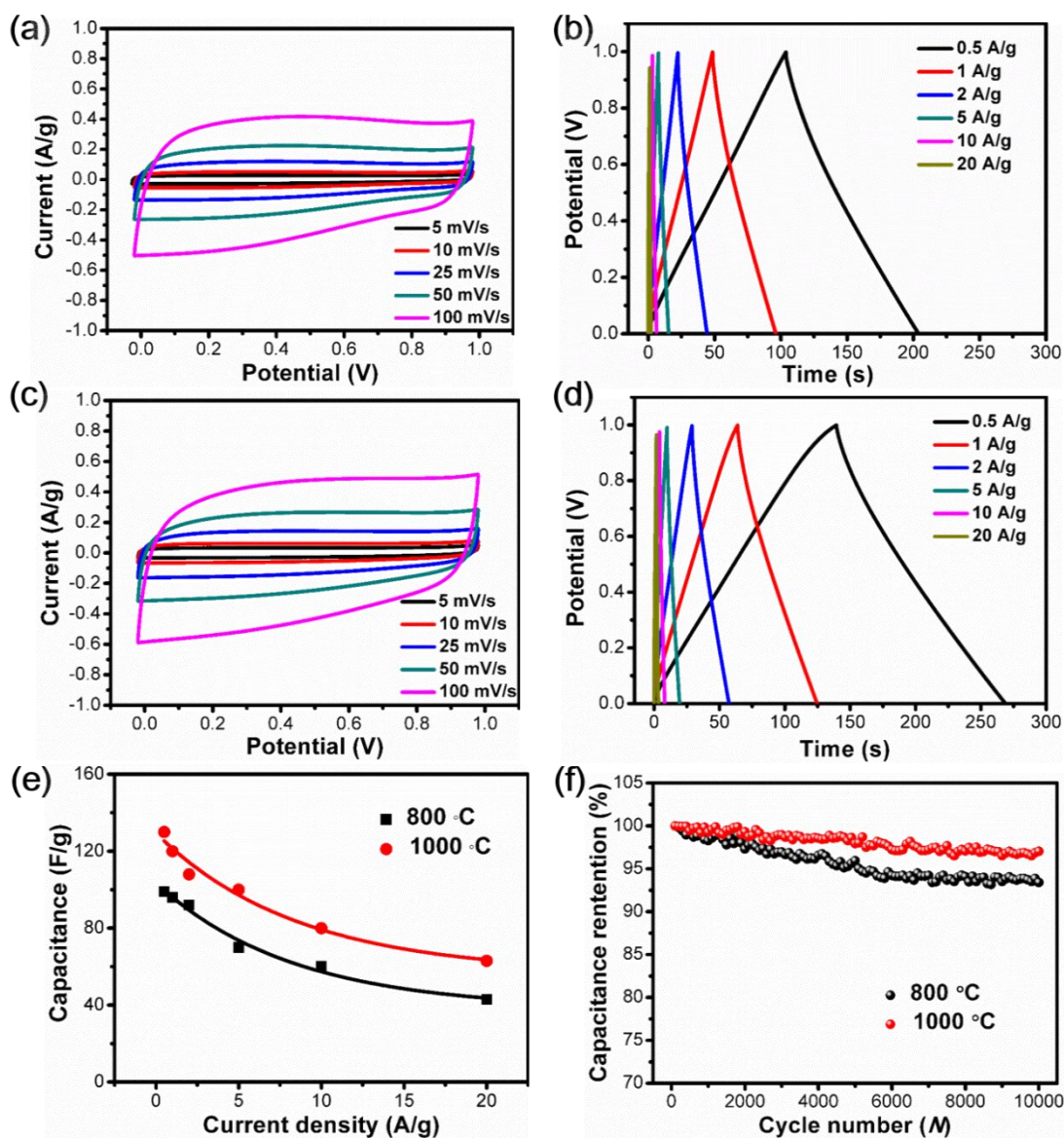


Figure 6. Typical (a) CV curves and (b) charge/discharge curves for PC-800; (c) CV curves and (d) charge/discharge curves for PC-1000; (e) Variation of capacitance as a function of current density for both materials; and (f) cyclic performance of the electrodes at 5 A/g.

The rate performance is important for supercapacitor, which was evaluated up to 20 A/g herein (Figure 6e). The capacitance decreased with the increase of current density due to the limited diffusion of ions at a higher current density. When the current reached 20 A/g, the capacitance of PC-800 still retained 43% of that measured at 0.5 A/g, and the capacitance retention is even higher, being 49% for PC-1000. The electrodes also demonstrated excellent cyclic stability. It can be seen from Figure 6f that

after 10000 cycles of charge/discharge at 5 A/g, PC-800 and PC-1000 still retained 93.4% and 97% of their initial capacitances, respectively. During the repeated charging/discharging, the graphitic structure could provide better stability than amorphous carbon due to its higher rigidity and electrical conductivity. These results manifest the advantages of graphitic structure both in electrocatalyst and supercapacitors.

EIS is a powerful technique to investigate the charge transfer both in the electrode and across the electrode/electrolyte interface. The Nyquist plots for the electrodes are shown in Figure 7. Nearly vertical lines are seen in the low frequency region in the plots, suggesting capacitive nature of these materials [21]. The solution resistance (R_s , which includes the resistance at the electrolyte/electrode interface) and charge transfer resistance (R_{ct}), can be determined from the intercept at the real axis and the diameter of the semicircle, respectively [21]. These values are 0.69 Ω and 2.19 Ω for PC-800 and 0.56 Ω and 0.36 Ω for PC-1000, respectively. These results also confirm the higher conductivity for the carbon treated at a higher temperature, which is responsible for the better performance in both ORR electrocatalyst and supercapacitor electrode.

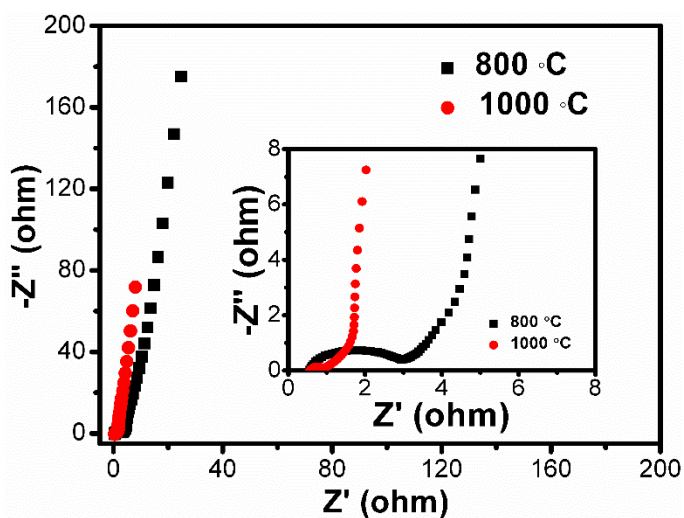


Figure 7. Impedance Nyquist plots for both PC-800 and PC-1000 electrodes (testing conditions: frequency range between 0.01 Hz and 10^6 Hz, and an open circuit voltage of 0.05 V).

4. CONCLUSIONS

Porous carbons with both large surface area and high degree of graphitization have been prepared by a one-pot pyrolysis of chitin in the presence of both FeCl_3 and ZnCl_2 . It was found the performances as electrocatalyst and supercapacitor electrode can be enhanced significantly by increasing the carbonization temperature from 800 $^\circ\text{C}$ to 1000 $^\circ\text{C}$. These improvements were attributed to the increase of specific surface area, as well as a higher degree of graphitization which improves the electrical conductivity and enhances the structural rigidity. The facile method for simultaneously achieving a high surface area and high degree of graphitization demonstrated in this study would pave the way for preparing multifunctional porous carbons from biomass and other low-cost and

environmental-friendly precursors, and would eventually foster the practical applications of these materials in energy storage and conversion.

ACKNOWLEDGEMENTS

This work was supported by Shenzhen Government's Plan of Science and Technology (KQJSCX2017033011014404), the National Natural Science Foundation of China (51602202 and 51702217), and the Chinese Postdoctoral Science Foundation (2017M612750).

References

1. J. Liu, N. P. Wickramaratne, S. Z. Qiao and M. Jaroniec, *Nat. Mater.*, 14 (2015) 763.
2. T. Lin, I.-W. Chen, F. Liu, C. Yang, H. Bi, F. Xu and F. Huang, *Science*, 350 (2015) 1508.
3. B.-H. Cheng, R. J. Zeng and H. Jiang, *Bioresour. Technol.*, 246 (2017) 224.
4. J. Deng, M. Li and Y. Wang, *Green Chem.*, 18 (2016) 4824.
5. Z. Sun, J. Liao, B. Sun, M. He, X. Pan, J. Zhu, C. Shi and Y. Jiang, *Int. J. Electrochem. Sci.*, 12 (2017) 12084.
6. Y. Yang, J. Zha, L. Liu and N. Yuan, *Int. J. Electrochem. Sci.*, 12 (2017) 7326
7. M. Borghei, J. Lehtonen, L. Liu and O. J. Rojas, *Adv. Mater.*, 29 (2017) 1703691.
8. S. Gao, H. Fan and S. Zhang, *J. Mater. Chem. A*, 2 (2014) 18263.
9. K. Chatterjee, M. Ashokkumar, H. Gullapalli, Y. Gong, R. Vajtai, P. Thanikaivelan and P. M. Ajayan, *Carbon*, 130 (2018) 645.
10. Y. Zhang, S. Liu, X. Zheng, X. Wang, Y. Xu, H. Tang, F. Kang, Q.-H. Yang and J. Luo, *Adv. Funct. Mater.*, 27 (2017) 1604687.
11. B. Hou, T. Zhang, R. Yan, D. Li, Y. Mo, L. Yin and Y. Chen, *Int. J. Electrochem. Sci.*, 11 (2016) 9007
12. M. Biswal, A. Banerjee, M. Deo and S. Ogale, *Energy Environ. Sci.*, 6 (2013) 1249.
13. Z. Tang, Z. Pei, Z. Wang, H. Li, J. Zeng, Z. Ruan, Y. Huang, M. Zhu, Q. Xue, J. Yu and C. Zhi, *Carbon*, 130 (2018) 532.
14. S. Dutta, A. Bhaumik and K. C.-W. Wu, *Energy Environ. Sci.*, 7 (2014) 3574.
15. N. Wang, T. Ling, J. Liu and F. Wang, *Carbon*, 130 (2018) 692.
16. D. Weingarth, M. Zeiger, N. Jäckel, M. Aslan, G. Feng and V. Presser, *Adv. Energy Mater.*, 4 (2014) 1400316.
17. L. Deng, H. Fang, P. Zhang, A. Abdelkader, X. Ren, Y. Li and N. Xied, *J. Electrochem. Soc.*, 163 (2016) H343.
18. J. Zhao, H. Lai, Z. Lyu, Y. Jiang, K. Xie, X. Wang, Q. Wu, L. Yang, Z. Jin, Y. Ma, J. Liu and Z. Hu, *Adv. Mater.*, 27 (2015) 3541.
19. J. Zhao, Y. Jiang, H. Fan, M. Liu, O. Zhuo, X. Wang, Q. Wu, L. Yang, Y. Ma and Z. Hu, *Adv. Mater.*, 29 (2017) 1604569.
20. W. Zhong, J. Chen, P. Zhang, L. Deng, L. Yao, X. Ren, Y. Li, H. Mi and L. Suna, *J. Mater. Chem. A*, 5 (2017) 16605.
21. L. Deng, W. Zhong, J. Wang, P. Zhang, H. Fang, L. Yao, X. Liu, X. Ren and Y. Li, *Electrochim. Acta*, 228 (2017) 398.
22. L. Yao, J. Yang, P. Zhang and L. Deng, *Bioresour. Technol.*, 256 (2018) 208.
23. L. Yao, Q. Wu, P. Zhang, J. Zhang, D. Wang, Y. Li, X. Ren, H. Mi, L. Deng and Z. Zheng, *Adv. Mater.*, 30 (2018) 1706054.
24. J. You, M. Li, B. Ding, X. Wu and C. Li, *Adv. Mater.*, 29 (2017) 1606895.
25. F. Caturla, M. Molina-Sabio and F. Rodríguez-Reinoso, *Carbon*, 29 (1991) 999.
26. L. Sun, C. Tian, M. Li, X. Meng, L. Wang, R. Wang, J. Yin and H. Fu, *J. Mater. Chem. A*, 1

- (2013) 6462.
27. L. Deng, R. J. Young, I. A. Kinloch, Y. Zhu and S. J. Eichhorn, *Carbon*, 58 (2013) 66.
28. Y. Li, H. Zhang, P. Liu, Y. Wang, H. Yang, Y. Li and H. Zhao, *Electrochem. Commun.*, 51 (2015) 6.
29. D. Gu, Y. Zhou, R. Ma, F. Wang, Q. Liu and J. Wang, *Nano-Micro Lett.*, 10 (2018) 29.
30. Y. Lu, G. Ye, X. She, S. Wang, D. Yang and Y. Yin, *ACS Sustainable Chem. Eng.*, 5 (2017) 8729.
31. Y. Chen, H. Wang, S. Ji, W. Lv and R. Wang, *Materials*, 10 (2017) 1366.
32. M. D. Stoller and R. S. Ruoff, *Energ Environ. Sci.*, 3 (2010) 1294.
33. R. Yan, T. Heil, V. Presser, R. Walczak, M. Antonietti and M. Oschatz, *Adv Sustainable Syst.*, 2 (2018) 1700128.
34. Y. Li, Q. Liu, W. Li, H. Meng, Y. Lu and C. Li, *ACS Appl. Mater. Interfaces*, 9 (2017) 3895.
35. M. Yu, Y. Han, J. Li and L. Wang, *Chem. Eng. J.*, 317 (2017) 493.
36. F.-C. Wu, R.-L. Tseng, C.-C. Hu and C.-C. Wang, *J. Power Sources*, 144 (2005) 302

© 2018 The Authors. Published by ESG (www.electrochemsci.org). This article is an open access article distributed under the terms and conditions of the Creative Commons Attribution license (<http://creativecommons.org/licenses/by/4.0/>).